

NEAR INFRARED OPTICAL TOMOGRAPHIC IMAGING OF FLUID CONTAINING TISSUES

A.H. Hielscher, G. Abdoulaev, A. Klose, A. Bluestone, J. Lasker

Depts. of Biomedical Engineering and Radiology, Columbia University,
500 West 120th Street, MC8904, New York, NY 10027

ABSTRACT

In recent years near-infrared optical tomographic imaging (OTI) has made big strides towards becoming a clinically relevant medical imaging modality. Imaging of dynamic changes in blood parameters, functional brain imaging, and breast imaging are the most advanced areas of application of this novel technique. In this study we focus on difficulties that are encountered when OTI is employed for imaging tissues that contain fluid-filled regions. Examples of such tissues are the brain, which contains low scattering cerebrospinal fluids, joints, which enclose translucent synovial fluids, and the maternal abdomen, which is filled with amniotic fluid. In these cases widely accepted image reconstruction schemes that rely on the diffusion approximation have limited applicability, and more advanced model-based iterative image reconstruction methods that make use of the equation of radiative transfer promise more accurate results.

1. INTRODUCTION

Since the mid nineties researchers have been working towards optical tomographic imaging systems that allow to get cross-sectional images from transmitted near-infrared light [1,2,3,4]. Implementing such a system presents some unique challenges, both with respect to the instrumentation and the numerical analysis of the data. On the instrument side one has to overcome the problem of a very large dynamic range, which is required to detect light intensities from a few mW down to pW [5,6,7]. When dealing with the image reconstruction problem one is faced with the fact that near-infrared photons, unlike X-rays, are highly scattered when they traverse the tissue from a source to a detector. Therefore, well-known backprojection algorithms have limited applicability and so-called model-based iterative image reconstruction schemes have emerged [8,9]. In these schemes a model of light propagation is used to predict measurements. By iteratively changing the tissue-parameters until the predictions agree with the real measurements, a spatial distribution of optical properties inside the tissue is found. If the model of light propagation is inaccurate, the reconstruction process will lead to an unreliable result. Most of the currently employed MOBIIR schemes rely on the diffusion theory. However, in areas where the tissue contains low scattering regions, diffusion theory has been shown to be

of limited applicability. [10,11] Examples for such regions are the cerebrospinal-fluid-filled space in the brain [12], the synovial-fluid-filled space in joints [13,14], or the amniotic fluid that surround the fetus in the uterus [15]. In these case it appears advantages to employ a transport equation based method. Our group has developed such algorithms in recent years [16,17,18] and is employing them now for the first time to *in vivo* studies with animals and humans. In this work we present our latest results on brain and joint imaging in human subjects.

2. INSTRUMENTATION

To acquire data we have used two types of instruments in our studies. When it is important to recover absolute optical properties, such as in the case of determining the scattering coefficient of the synovial fluid, one has to perform optical measurement in a way that for each light source the values of all detector readings are known with respect to each other. In this case we employed a setup as shown in Fig. 1. One complete data set for the image reconstruction is obtained by fixing the position of the laser diode, taking multiple detector readings by moving the photodiode over the whole range of the measurement window, fixing the laser diode at another position, again taking multiple detector readings by moving photodiode over the whole range of the measurement window, etc.. While time consuming, this process provides the most accurate measurements. A detailed description of the system can be found in ref. [16].

A second type of instrument is used when it is sufficient to locate changes in the optical properties, instead of absolute values. This is, for example, the cases in functional imaging when changes in blood oxygenation and blood deoxygenation are of interest, similar to functional magnetic

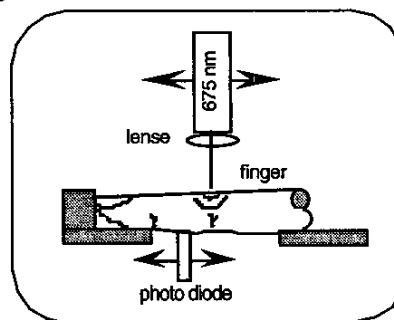


Fig.1: Experimental setup for joint imaging.

resonance imaging (MRI). While absolute values are also desirable in this case, the time required for the necessary data acquisition is currently still too long. To allow observing fast changes, fast data acquisition is necessary, and optical imaging systems are employed, that acquire signals from multiple detector position simultaneously. For the brain studies in this work we use a dynamic optical imaging system developed by Schmitz et al. [5]. The beam from two continuous-wave laser diodes with wavelengths of $\lambda = 760\text{nm}$ and $\lambda = 830\text{nm}$, respectively, are coupled into a set of source fiber bundles. Having this two-wavelength capability allows for the elucidation of both oxyhemoglobin and deoxyhemoglobin. For the measurements presented in this work we used 4 sources and 15 detectors, resulting in 60 source-detector combinations. Three full tomographic data sets, involving all 60 source-detector pairs, were acquired per second. A more detailed description of the system can be found elsewhere [5].

3. IMAGE RECONSTRUCTION SCHEME

Once the data are acquired, they are input into a model-based iterative image reconstruction (MOBIIR) scheme. The goal of the MOBIIR scheme is to reconstruct the distribution of the optical properties inside a medium, from a given set M of measurements on the circumference, $\partial\Omega$, of the medium. One can divide the MOBIIR scheme in 3 different major components: (1) *Forward Model*: This model is a theory or algorithm that predicts a set of measured signals, based on the position of the light source and the spatial distribution of optical properties $\zeta = (\mu_a(r), \mu_s(r))$, where μ_a and μ_s are the absorption and scattering coefficient, respectively. (2) *Analysis Scheme*: Here an objective function, ϕ , is defined, which describes the difference between the measured, M , and predicted data, M_p . A simple example is the least-square error norm $\phi(\zeta) \sim (M - M_p(\zeta))^2$. Since the problem is highly ill-posed, a regularization term, R , is usually added to the objective function. (3) *Updating Scheme*: Once the objective function is defined, the task becomes to minimize ϕ . This is accomplished in two substeps: (3a) First, the gradient of the objective function $d\phi(\zeta)/d\zeta$ is calculated by means of so-called adjoint differentiation. The effective calculation of this gradient poses a major challenge in itself and is described in detail elsewhere. (3b) Second, given the gradient an iterative line minimization in the direction of the gradient is performed, which consists of several forward calculations in which the optical parameters ζ are varied. Once the minimum along the line is found, a new gradient is calculated and another line-minimization is performed, now along a different direction. These steps are repeated until a distribution ζ is found for which $\phi(\zeta)$ is smallest.

We have developed several MOBIIR algorithms that employ different forward models, based on the diffusion equation as well as the equation of radiative transfer. Both finite-element and finite-difference implementation have been tested.

4. EXPERIMENTAL RESULTS

4.1. Dynamic Brain Imaging

Using the instrumentation and algorithm just described we have performed initial brain as well as joint imaging studies.

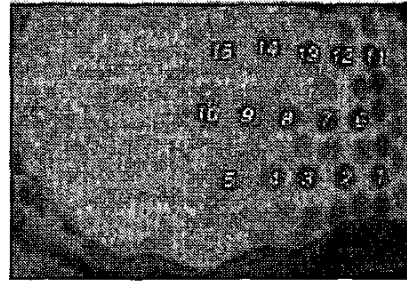


Fig. 2: Photo of the forehead with numbered locations of optical sources and detectors.

Our experiment was designed to look at hemodynamic changes in the human forehead induced by a Valsalva maneuver. For the measurement the subject was placed in the supine position. Three epochs consisting of Valsalva maneuvers with one-minute rest periods interspersed were performed. During the Valsalva maneuver a forced expiration against a closed glottis demonstrates the effects of changes in intrathoracic pressure on blood pressure, and the brain's autoregulatory response to decreased vascular perfusion pressure in cerebral vessels. Figure 2 shows the locations of the sources and detectors on the forehead.

A trace of the measured output produced by the optical image system for one Valsalva epochs is shown in Fig. 3. Displayed are selected signal traces for source at position #3 and detectors at positions #1, 3, 5, 7, 11, 13, and 15 (see Fig. 1). Each trace is normalized to the rest period before the Valsalva maneuver started. It can be seen that the Valsalva maneuver produces a strong signal drop in all detectors. At the peak of the Valsalva maneuver the measurement intensities changed with respect to the rest period by almost 40%.

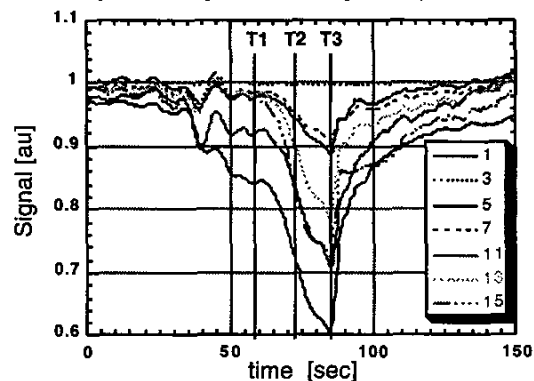


Fig. 3. Changes in the detector signals during a Valsalva maneuver for a source located at position #3 (see fig. 2) and selected detector positions. The wavelength of the source was $\lambda = 760\text{nm}$.

For the "difference" reconstruction we used the ratio of the data at the time points T1, T2, and T3, with respect to data at time point $t = 0$ (Fig. 3). Figures 4-6 show the three-dimensional distribution of the reconstructed values for changes in deoxyhemoglobin (Hb) and oxyhemoglobin (HbO₂) at all three time points. All reconstructions were stopped after 25 iterations. The 25 iterations for each image took approximately 1 hours on a Pentium III 550Mhz processor. Displayed are volumetric reconstructions for three different views: frontal (standing in front of body and

looking towards the face), side (standing next to body and looking towards the right ear), and aerial (looking from top of the head down towards the body). The different colors (shadings) represent isosurfaces of constant oxyhemoglobin and deoxyhemoglobin concentration changes relative to the reference point at $t = 0$.

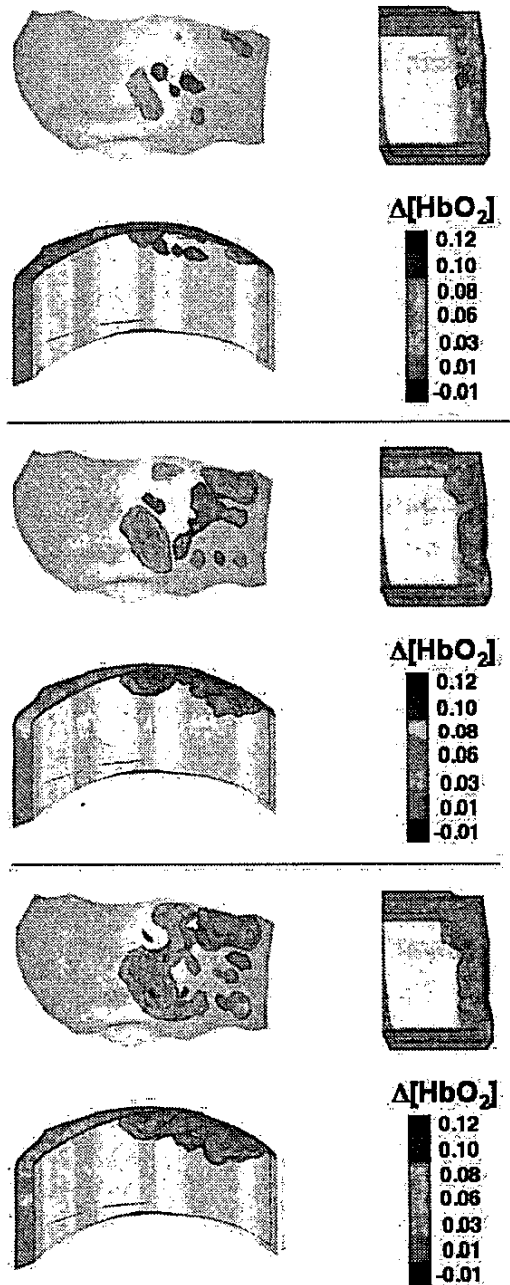


Fig. 4: Reconstructed changes in HbO_2 (top) at time T_1 , T_2 , and T_3 (see Fig.3) during a Valsalva maneuver. The changes are given in units of [mM]. Shown are a frontal view (upper left), a side view (upper right), and an aerial or birds-eye view (lower left) of the forehead.

4.2. Joint Imaging

For the diagnosis of rheumatoid arthritis it is of particular importance to determine the changes in the optical properties of the synovial fluid and the synovium. These changes are dominated by changes in the scattering coefficient. To obtain these optical properties one cannot rely on dynamic changes, but needs to reconstruct absolute values. A total of 8 volunteers with RA in stage II were recruited and informed consent was obtained prior to the study. All of the subjects were diagnosed with RA in at least one of the interphalangeal PIP joint of one hand, while the same joint in the contra-lateral hand was found to be not affected. Optical trans-illumination measurements were performed on the same joint of both hands.

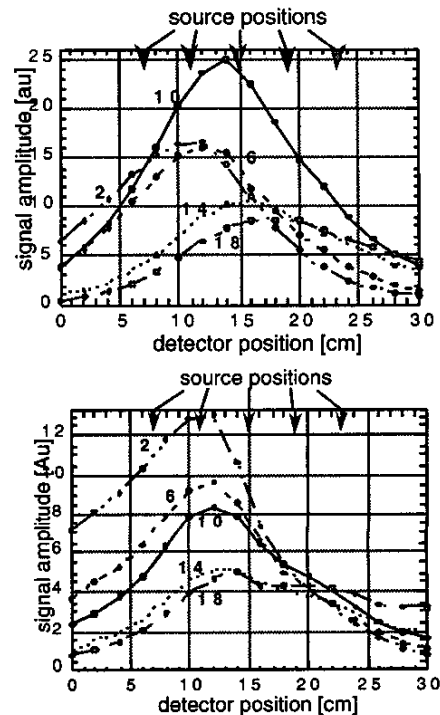


Fig. 5: Intensity transmission profiles for 5 different source positions for a healthy joint (left) and the same joint on the contra lateral hand with rheumatoid arthritis (right). Source position 2 is closest to the finger tip, while source position 18 is furthest from the finger tip. Source position #10 is located directly above the PIP joint.

We found significant differences in the sagittal trans-illumination data between the healthy joint and the joint with symptoms of RA. An example of a set of measurements from a subject is shown in Figs. 5a and 5b. In both figures trans-illumination curves for 5 different source positions, which are indicated by the arrows, are shown. Source position 2 is closest to the finger tip, while source position 18 is furthest from the finger tip. In Fig. 5a, which illustrates a measurement on a healthy joint, the trans-illumination data for the source #10, clearly shows the strongest transmission signal. In Fig. 5b, which shows measurements on a rheumatoid joint, measurements at source position #10 don't show such a strong signal.

In another experiment, a full tomographic data set obtained during a cuff experiment was used to generate images of the distribution of changes in the optical properties. A cross-sectional image of the distribution of absorption-coefficient changes is shown in Fig 3. It clearly can be seen that changes take place in tissue areas surrounding the joint, rather than in the joint itself. The increase is highest at the interior base of the finger and moderate around the outer perimeter. This behavior is expected since it reflects the distribution of blood vessels inside the finger. A buildup of venous blood in the finger should lead to an increase in the absorption coefficient mainly in areas occupied by blood vessels. Regions occupied by synovial fluid, cartilage and bones show little change during an arm cuff experiment.

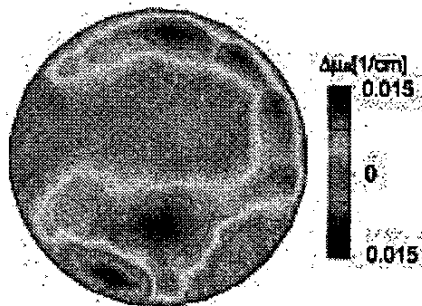


Fig. 6. Cross-section of changes in absorption coefficient in an around a PIP finger joint during a cuff experiment.

5. SUMMARY

In recent years, Optical tomographic imaging has emerged as a novel biomedical imaging method. Several groups apply this technology in first clinical studies which look to proof utility, for example, in areas such as breast imaging, brain imaging, and fetal monitoring. In this work we focused on the application of OTI for imaging tissues that contain low scattering fluids, such as the cerebrospinal fluid in the head or the synovial fluid in joints. In these case diffusion-theory based reconstruction models have limited applicability and transport-theory-based iterative image reconstruction schemes promise more accurate results. We have developed such algorithms and applied them to imaging problems related to vascular reactivity in the human forehead and detection of rheumatoid arthritis in finger joints. We showed that we can detect and localize changes in oxy and deoxyhemoglobin in the human forehead during Valsalva maneuvers. We were also able to obtain reconstructions of the optical properties in human finger joints. While the first results are encouraging more work needs to be done to conclusively validate the algorithms and prove diagnostic utility of optical tomographic imaging.

6. ACKNOWLEDGEMENTS

We would like to thank Prof. R. Barbour and Dr. C. Schmitz, SUNY Downstate Medical Center, for providing time and assistance with the near-infrared DYNOT imaging system. Thanks also to Prof. J. Beuthan and U. Netz from the Laser Medicine Centrum at the Free University Berlin, for their help with the cw imaging system. This work was supported in part by the National Institute of Arthritis and Musculoskeletal

and Skin Diseases, a part of the National Institutes of Health (NIH) (grant # R01 AR46255-02), an SBIR grant (2R44-HL-61057-02) from the National Heart, Lung, and Blood Institute at NIH, the New York City Council Speaker's Fund for Biomedical Research, and the Whitaker Foundation for Biomedical Research (grant # 98-0244).

7. REFERENCES

- [1] B. Chance, R.R. Alfano, and A. Katzirels, eds., *Optical Tomography, Photon Migration, and Spectroscopy of Tissue and Model Media: Theory, Human Studies, and instrumentation*, SPIE Proc. 2389, Bellingham, WA, 1995.
- [2] B. Chance, R.R. Alfano, and A. Katzirels, eds., *Optical Tomography, Photon Migration, and Spectroscopy of Tissue and Model Media: Theory, Human Studies, and instrumentation II*, SPIE Proc. 2979, Bellingham, WA, 1997.
- [3] B. Chance, R.R. Alfano, B.J. Tromberg, and A. Katzirels, eds., *Optical Tomography, Photon Migration, and Spectroscopy of Tissue III*, SPIE Proc. 3597, Bellingham, WA, 1999.
- [4] B. Chance, R.R. Alfano, B.J. Tromberg, M. Tamura, and E.M. Sevick-Muraca, eds., *Optical Tomography, Photon Migration, and Spectroscopy of Tissue III*, SPIE Proc. 4250, Bellingham, WA, 2001.
- [5] C.H. Schmitz, Y. Pei, H.L. Graber, J.M. Lasker, A.H. Hielscher, R.L. Barbour, "Instrumentation for real-time dynamic optical tomography," in *Photon Migration, Optical Coherence Tomography, and Microscopy*, S. Andersson-Engels, M.F. Kaschke, eds., SPIE Proc. 4431, pp. 282-291, 2001.
- [6] A. M. Siegel, J. J. A. Marota, and D. A. Boas, "Design and evaluation of a continuous-wave diffuse optical tomography system," *Opt. Exp.* Vol. 4, 287-298 (1999).
- [7] J. C. Hebden, S. R. Arridge, and D. T. Delpy, "Optical in imaging in med. I: Experimental techniques," *Phys. Med. Biol.* 42, 825-840 (1997).
- [8] A.H. Hielscher, A.D. Klose, K.M. Hanson, "Gradient-based iterative image reconstruction scheme for time-resolved optical tomography," *IEEE Trans. on Medical Imaging* 18, pp. 262-271, 1999.
- [9] S.R. Arridge, "Optical tomography in medical imaging," *Inverse Problems* 15, pp. R41-R93 (1999).
- [10] A.H. Hielscher, R.E. Alcouffe, R.L. Barbour, "Comparison of finite-difference transport and diffusion calculations for photon migration in homogeneous and heterogeneous tissues," *Phys. Med. Biol.* 43, pp. 1285-1302, 1998.
- [11] H. Dehghani, D.T. Delpy, and S.R. Arridge, "Photon migration in non-scattering tissue and the effects on image reconstruction," *Phys. Med. Biol.* 44(12), pp. 2897-2906, 1999.
- [12] A.Y. Bluestone, G. Abdoulaev, C. Schmitz, R.L. Barbour, A.H. Hielscher, "Three-dimensional optical-tomography of hemodynamics in the human head", *Optics Express* 9(6), pp. 272-286, 2001.
- [13] U. Netz, J. Beuthan, H.J. Capius, H.C. Koch, A.D. Klose, A.H. Hielscher, "Imaging of rheumatoid arthritis in finger joints by sagittal optical tomography," *Medical Laser Application* 16, pp. 306-310, 2001.
- [14] A. Klose, A.H. Hielscher, K.M. Hanson, J. Beuthan, "Three-dimensional optical tomography of a finger joint model for diagnostic of rheumatoid arthritis," *SPIE Proc.* 3566, pp. 151-160, 1998.
- [15] N. Ramanujam, G. Vishnoi, A.H. Hielscher, M. Rode, I. Forouzan, and B. Chance, "Photon migration through the fetal head in utero using continuous wave, near infrared spectroscopy: Clinical and experimental model studies," *J. of Biomedical Optics* 5, pp. 173-184, 2000.
- [16] A.D. Klose, U. Netz, J. Beuthan, and A.H. Hielscher, "Optical tomography using the time-independent equation of radiative transfer. Part I: Forward model," *J. Quant. Spect. & Rad. Trans.*, Vol 72/5, pp 691-713, 2002.
- [17] A.D. Klose and A.H. Hielscher, "Optical tomography using the time-independent equation of radiative transfer. Part 2: Inverse model," *J. Quant. Spect. & Rad. Trans.*, Vol 72/5, pp 715-732, 2002.
- [18] G. Abdoulaev, A. Klose, A. Bluestone, A.H. Hielscher, "Three-dimensional optical tomography based on the even-parity finite-element formulation of the radiative transfer equation," in *Optical Tomography and Spectroscopy of Tissue IV*, B. Chance et al, eds., SPIE Proc. 4250, pp. 53-60, 2001.